Supporting Information for

Homoleptic Alkynyl-Protected $[Ag_9Cu_6(^tBuC{\equiv}C)_{12}]^+$ Superatom with Free Electron: Synthesis, Structure Analysis, and Different Properties with Au_7Ag_8 Cluster in the M_{15}^+ Series

Xiaoshuang Ma,‡[a] Lin Xiong,‡[b] Lubing Qin,[a] Yun Tang,[a] Guanyu Ma,[a] Yong Pei,*[b] and Zhenghua Tang*[a]

[a] Guangzhou Key Laboratory for Surface Chemistry of Energy Materials and New Energy Research Institute, School of Environment and Energy, South China University of Technology, Guangzhou Higher Education Mega Centre, Guangzhou, Guangdong, 510006 (P. R. China).
E-mail: zhht@scut.edu.cn

[b] b. Department of Chemistry, Key Laboratory of Environmentally Friendly Chemistry and Applications of Ministry of Education, Xiangtan University, Hunan Province, Xiangtan 411105 (P. R. China).
E-mail: ypei2@xtu.edu.cn.

‡ X. Ma and L. Xiong contributed equally to this work.

Table of Contents

Experimental Procedures

I. Synthesis.

Materials and Reagent: Dichloromethane (DCM), ethanol (EtOH), methanol (MeOH), acetonitrile (MeCN), diethyl ether, and ethyl acetate (EA) were purchased from Caiyunfei Chemical Reagents (Tianjin, China). 3, 3-dimethyl-1-butyne (^{t}BuC≡CH, 96%), triphenylphosphine (PPh_3, 98%), anhydrous dimethyl sulfide (Me_2S, 99.0%), anhydrous triethylamine (Et_3N, 99.5%), ammonium hydroxide ($NH_3{\cdot}H_2O$: 28.0 ~ 30.0% NH_3), silver(I) oxide (Ag_2O, 99.0%), sodium hexafluoroantimonate(V) ($NaSbF_6$, 99.0%), copper(I) chloride (CuCl, 98%), and hydrogen tetrachloroaurate (III) trihydrate ($HAuCl_4{\cdot}3H_2O$, Au 50%) were acquired from Energy Chemicals (Shanghai, China). Sodium borohydride ($NaBH_4$, 98%) was obtained from Aladdin Industrial Corporation (Shanghai, China). The water with the resistivity of 18.3 $M\Omega{\cdot}cm^{-1}$ was supplied by using a Barnstead Nanopure water system. All chemicals were used as received without further purification.

Synthesis of the ^{t}BuC≡CAg(I): ^{t}BuC≡CAg(I) was synthesized according to a reported protocol with some minor modifications.[1] Briefly, Ag_2O (500 mg, 2.1 mmol) was added into a 50 mL flask first, and 20 mL ammonium hydroxide ($NH_3{\cdot}H_2O$) was introduced. The mixture was kept vigorously stirring for approximately 10 min until the black solid dissolves to form a colorless solution, and then the solution was filtered. 5 mL deionized water was added to the above filtrate (silver ammonia solution: $Ag(NH_3)_2OH$) under stirring. After 5 min, 3, 3-dimethyl-1-butyne (950 mg, 4.1 mmol in 2.5 mL of ethanol) was added dropwise (in 10 min) under vigorous stirring (1000 rpm). The colorless solution immediately forms a white precipitate. After that, the crude products were washed with excess deionized water, ethanol (3 × 10 mL), and diethyl ether (2 × 10 mL), and then collected by centrifugation to give ^{t}BuC≡CAg(I). The product was a white solid without drying (yield: 95 %).

Synthesis of $[Ag_9Cu_6(C_6H_9)_{12}]SbF_6$ nanocluster (NC 1): In a typical synthesis, ^{t}BuC≡CAg precursor was directly reduced with $(PPh_3)_2CuBH_4$. Briefly, ^{t}BuC≡CAg (6.30 mg, 0.03 mmol) and $NaSbF_6$ (7.84 mg, 0.03 mmol) were co-dispersed in 6 mL mixed solvents of dichloromethane and acetonitrile (V_{DCM}: V_{MeCN} = 2: 1) under the ultrasound condition at room temperature (160 W, 40 kHz). After 10 min, a freshly prepared $(PPh_3)_2CuBH_4$ (0.06 mmol in 2 mL of dichloromethane) solution was directly added into the above solution under vigorous stirring (800 rpm) for 10 min. The solution changed from colorless to yellow and finally to dark brown. The solution was then hatched 12 h in the absence of light. After that, the blue solution was evaporated to give a black solid, which was successively washed with excess ethyl acetate and methanol to remove the by-products and inorganic salt, followed by extraction with dichloromethane and then dried by rotary evaporation. After diffusion of methanol to a dichloromethane solution at 10 °C for about one week, block-like blue crystals were obtained (yield: 41.05 % based on Ag).

Synthesis of $[Ag_8Au_7(^t$BuC≡C$)_{12}]SbF_6$ nanocluster (NC 2): Firstly, $Au_{22}(^t$BuC≡C$)_{18}$ clusters were synthesized following the methods reported by us previously.[2] Then, the Au_7Ag_8 clusters could be synthesized by an anti-galvanic reaction. 5 mg of $Au_{22}(^t$BuC≡C$)_{18}$ was first dissolved in 5 mL dichloromethane and acetonitrile. Freshly prepared acetonitrile solution (1 mL) containing 2 equivalents of ^{t}BuC≡CAg(I) complex and 1 equivalent of $NaNO_3$ was added into the DCM solution under vigorous stirring for 36 h in the absence of light. After the reaction was completed, the

reaction mixture was concentrated by evaporating the solvent under reduced pressure. The crude products dissolved in 1 mL of DCM were pipetted onto ten pieces of a preparative thin layer chromatography (PTLC) plate (10 cm by 20 cm), and the separation was conducted in a developing tank (solvent: DCM /n-hexane = 1: 1, volume ratio) for ~10 min. Then, the band of Au_7Ag_8 in the PTLC plate was cut, and the nanoclusters were extracted with pure DCM and then dried by rotary evaporation. After diffusion of *n*-hexane to a dichloromethane solution at 4 ^oC for about 7 days, red block crystals were obtained (yield: ca. 86.72 % based on Au).

II. Measurements and instrumentation.

The chemical compositions and valence states of the samples were examined by X-ray photoelectron spectroscopy (XPS, Phi X-tool instrument). UV-visible (UV-Vis) absorption spectra were recorded on a Shimadzu 2600/2700 spectrophotometer (Japan).

III. Electrospray ionization mass spectrometry (ESI-MS)

The ESI-MS spectra of the two title NCs were acquired on a Bruker UItiMate 3000 time-of-flight (TOF) system. ESI-MS instrumental parameters were maintained at the following values: capillary voltage, -3.5 kV; Dry temp, 200 ^oC; Nebulizer, 0.6 bar; Dry gas, 6.01 mL/min. The ESI sample was dissolved in dichloromethane (~1 mg/mL). All the mass spectra were obtained with positive ion mode. Calibration was performed using CsI clusters.

IV. X-ray Crystallography

Data collection for $[Ag_9Cu_6(C_6H_9)_{12}]SbF_6$ and $[Au_7Ag_8(C_6H_9)_{12}]SbF_6$ were carried on an Agilent Technologies SuperNova Single Crystal Diffractometer using Cu K_α radiation (λ = 1.54178 Å) at 100 K. Absorption corrections were applied by using the program CrysAlis (multi-scan).3 Structure solution was carried out using SHELXT and refinement with SHELXL, within the OLEX2 graphical interface.[3-5] All non-hydrogen atoms were refined first isotropically and then anisotropically. All the hydrogen atoms of the ligands were placed in calculated positions with fixed isotropic thermal parameters and included in the structure factor calculations in the final stage of full-matrix least-squares refinement. Detailed crystal data and structure refinements for the molecule are given in Table S1 and Table S2. CCDC 2044223 and 2072510 for $[Ag_9Cu_6(C_6H_9)_{12}]SbF_6$ and $[Au_7Ag_8(C_6H_9)_{12}]SbF_6$ contain the supplementary crystallographic data for this paper. These data are provided free of charge by the Cambridge Crystallographic Data Centre.

V. Computational details

In this work, the structure optimization is based on the Dmol^3 module [6, 7] using density functional theory (DFT) without any simplification of the clusters. The Perdew–Burke–Ernzerhof (PBE) functional[8] and the *d*-polarization basis set (DND) was used for the elements C and H. The DFT semi-core pseudopotential (DSPP) approximation with some degree of relativistic correction into the core was used for Au, Ag and Cu implemented in the Dmol^3 package. In addition, since both clusters contain considerable flexible organic ligands such as ^{t}BuC≡C, we use the Tkatchenko and Scheffler method[9] to consider possible weak interactions (such as dispersion effects) in the molecule to improve the calculation accuracy. After that, the calculations of vibration frequency were based on optimized structures with minimum energy point. The molecular orbital diagrams were visualized using Materials Studio software, and the value of the isosurface is set to 0.002.

The time-dependent DFT (TD-DFT) and Kohn-Sham (KS) molecular orbital energy level as implemented in Amsterdam Density Functional (ADF) software package[10] was utilized for calculating the ultraviolet–visible (UV–Vis) spectra of the two clusters. The triple-zeta polarized (TZP) basis set with inclusion of the scalar relativistic effect via a zeroth-order regular approximation (ZORA) implemented in the ADF package was adopted. The TD-DFT calculations evaluated the lowest 800 singlet-to-singlet excitation energies.

Supporting Figures

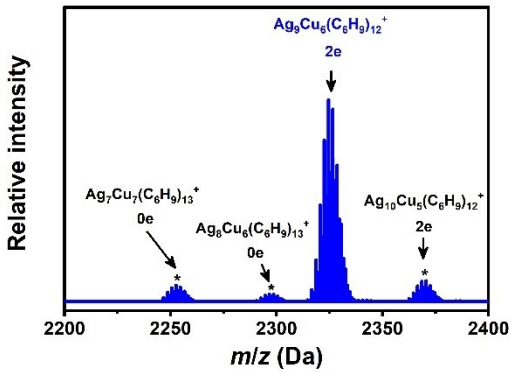

Figure S1. The analysis of fragment in the ESI-MS spectra of NC **1**. The local enlarged view of ESI-MS of NC **1** from 2200 to 2400 Da, the asterisks (*) indicate the fragment ions of NC **1**.

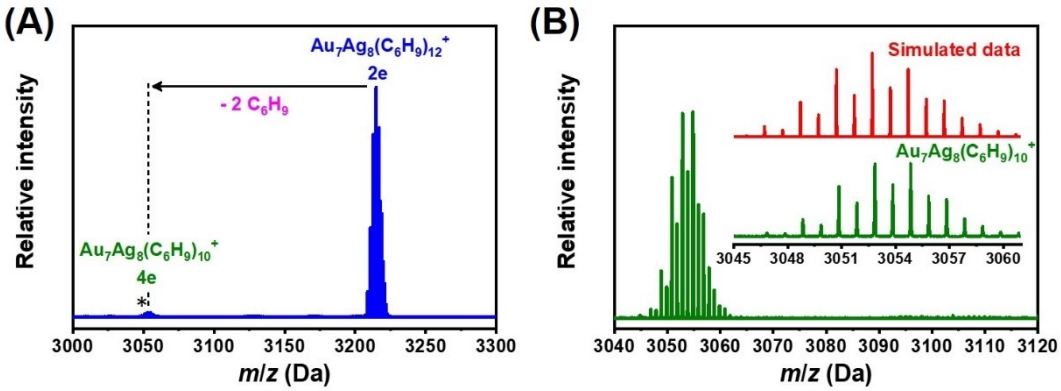

Figure S2. The analysis of fragment in the ESI-MS spectra of NC **2**. (A) The local enlarged view of ESI-MS of NC **2**, the asterisk (*) indicates the fragment ion of NC **2**, which was generated by losing two ligands ($-C_6H_9$) from parent NC **2**. (B) The experimental isotopic pattern (green) and simulated (red) data of NC **2**.

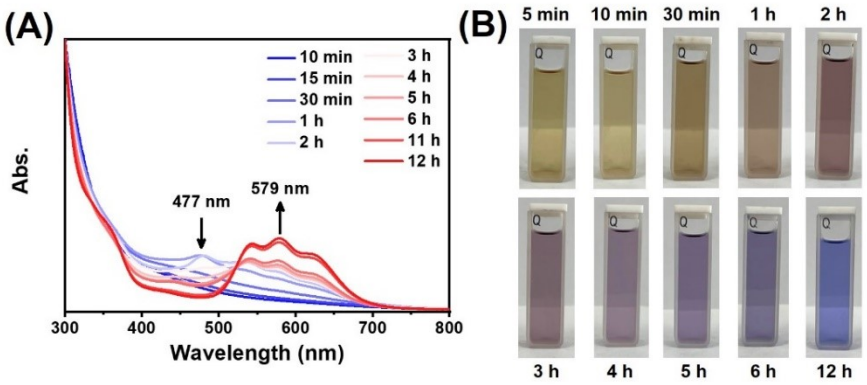

Figure S3. The in-situ monitoring of the content change during the formation process of NC **1**. (A) Time resolved UV-vis absorption spectra (from the precursor to the reaction mixture at 12 h after adding $(PPh_3)_2CuBH_4$), (B) the reaction solution with digital photos.

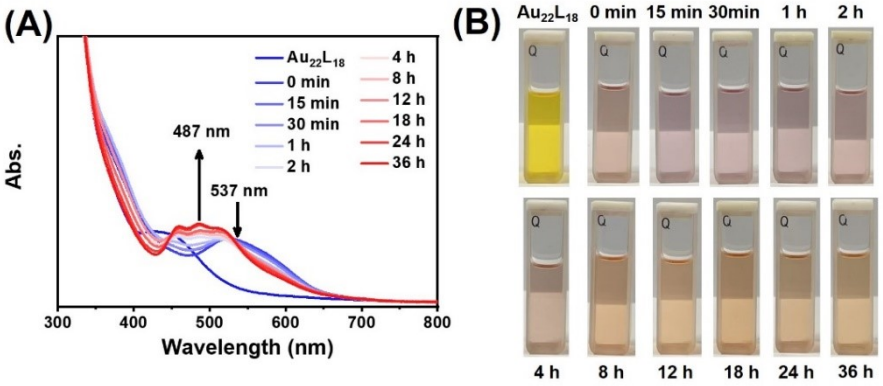

Figure S4. The in-situ monitoring of the content change during the formation process of NC **2**. (A) Time resolved UV−vis absorption spectra (from $Au_{22}(^t BuC{\equiv}C)_{18}$ to the reaction mixture at 36 h after adding $^t BuC{\equiv}CAg(I)$), (B) the reaction solution with digital photos.

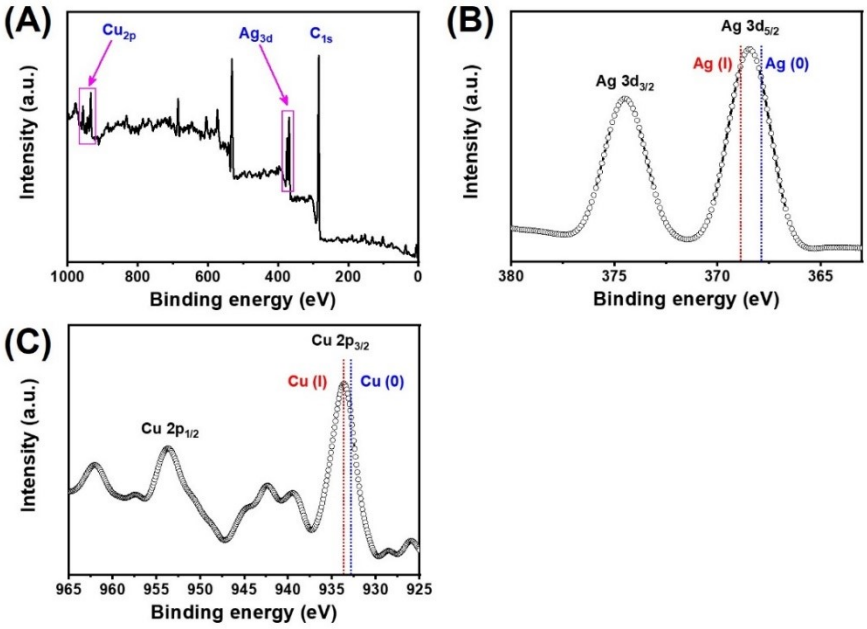

Figure S5. XPS survey scan spectra (A), core-level XPS spectra of the Ag 3d (B) and Cu 2p (C) electrons in NC **1**. The binding energy was calibrated based on the C 1s peak at 284.5 eV.

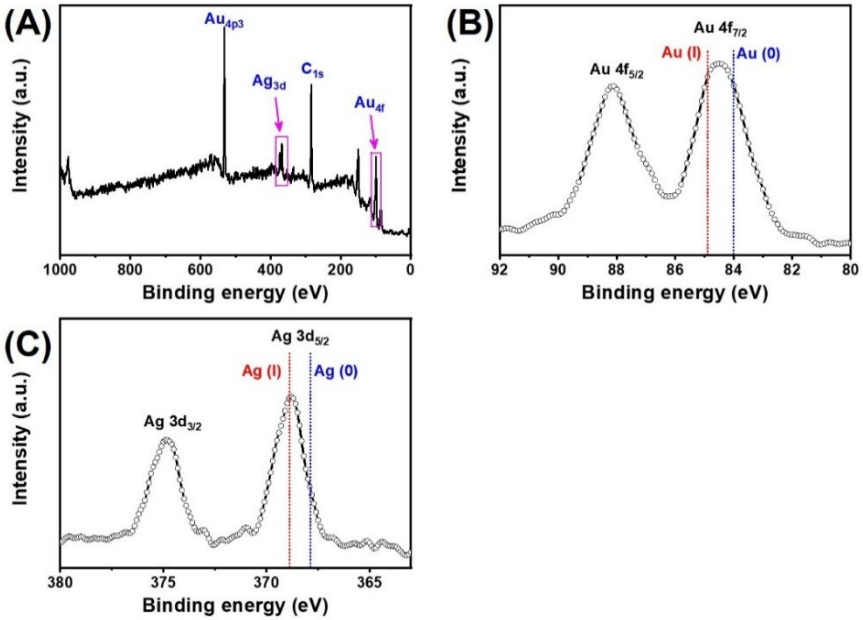

Figure S6. XPS survey scan spectra (A), core-level XPS spectra of the Au 4f (B) and Ag 3d (C) electrons in NC **2**. The binding energy was calibrated based on the C 1s peak at 284.5 eV.

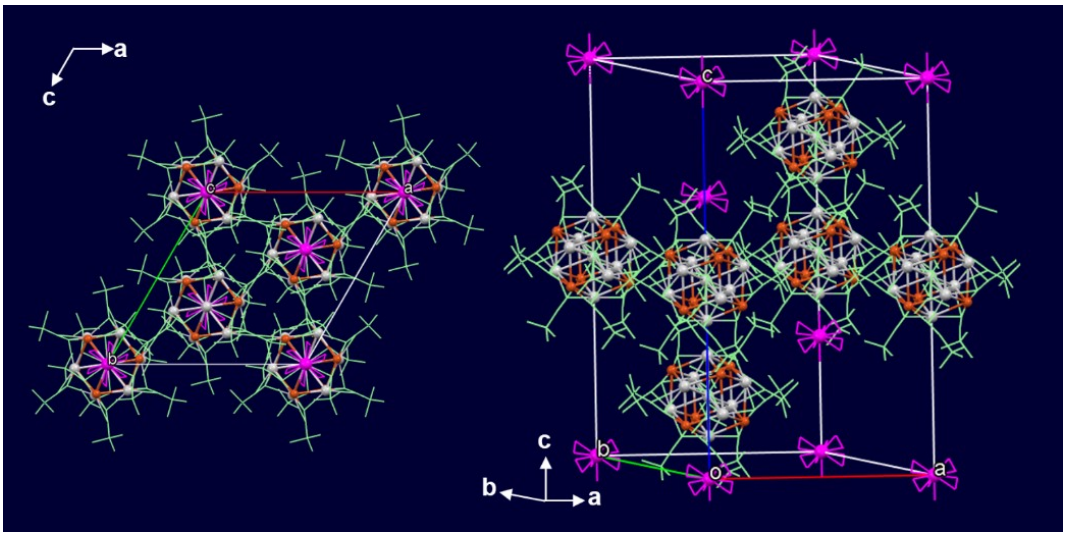

Figure S7. The top (left) and side (right) views of crystal packing structure of NC **1** with SbF_6^-. The SbF_6^- anions are highlighted in magenta for better visualization. Color legend: Cu, orange sphere; Ag, light grey sphere; C, dark grey stick; hydrogen atoms are omitted for clarity.

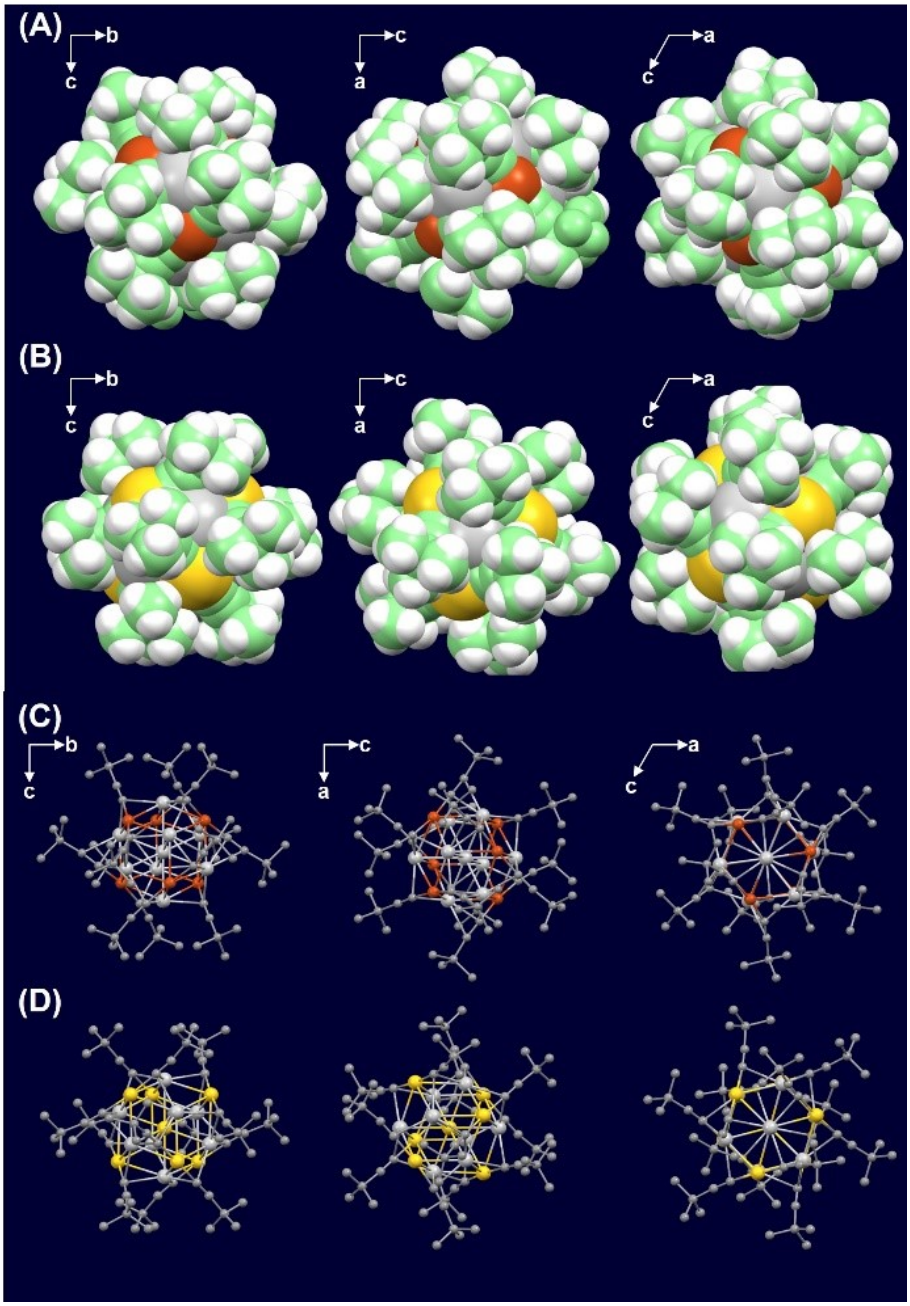

Figure S8. The structural comparison between NCs **1** (A for space-filling, and B for ball-and-stick model) and **2** (C for space-filling, and D for ball-stick model) in views along *a*-axis (left), *b*-axis (middle), and *c*-axis (right).

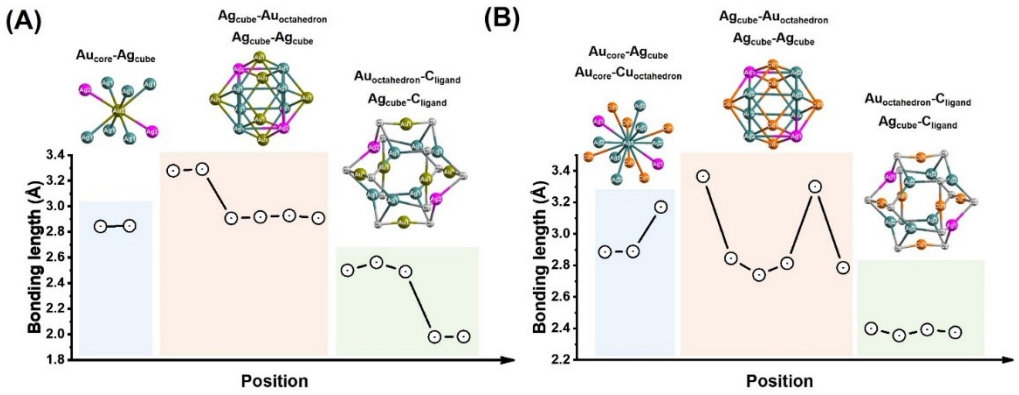

Figure S9. Lengths of bonds spread on different layer of $M_{core}@M_{cube}@M_{octahedron}$ structure in NCs **1** (A) and **2** (B). Note that, the Ag_8 cube was distorted by two Ag atoms located on the vertex. Color label: yellow = gold; cyan, fuchsia = silver; orange = copper; gray = carbon.

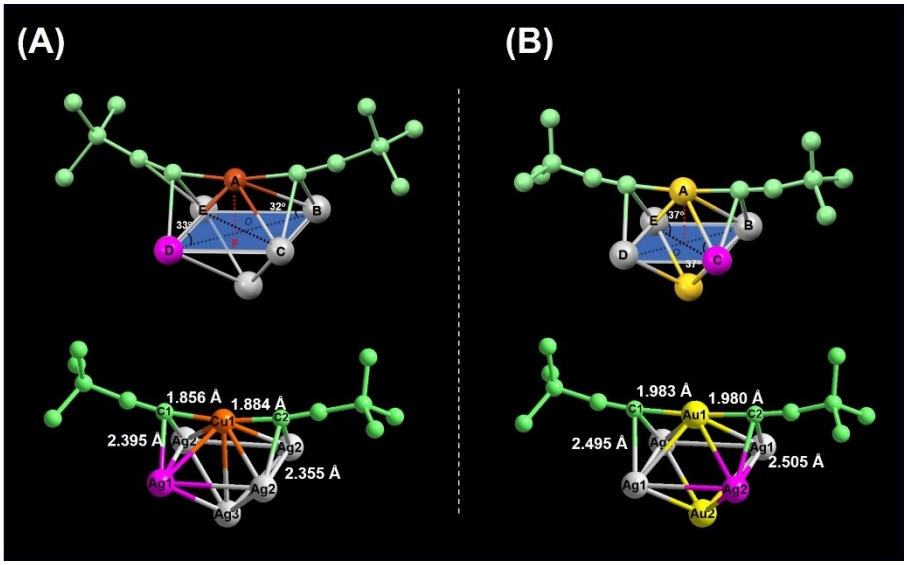

Figure S10. The structure analysis of the (A) Cu-capped $CuAg_4$ tetragonal pyramids and (B) Au-capped $AuAg_4$ tetragonal pyramids. The segment AB (Cu1-Ag2 distance) was 2.8454 Å, however, the segment AD (Cu1-Ag1 distance) was 2.7855 Å. After calculation, the segment OB of 2.371 Å (OB= AB × cos∠ABO = 2.8454 (Å) × cos 32^o = 2.4130 (Å)) was a little bit larger than half of the Ag_4 bottom diagonal (OE=OC= 2.3441 Å), signifying the capped Cu atom isn't located above the center of the Ag_4 bottom and the projection of the capped Cu atom is located at *F* of the Ag_4 bottom. However, in NC **2**, the ∠ACO = ∠AEO is 37^o, indicating that the projection of the capped Au atom is located at *O* of the Ag_4 bottom. The capped Au atom located above the center of the Ag_4 bottom, which was in accord with the results reported by Wang et al.[11]

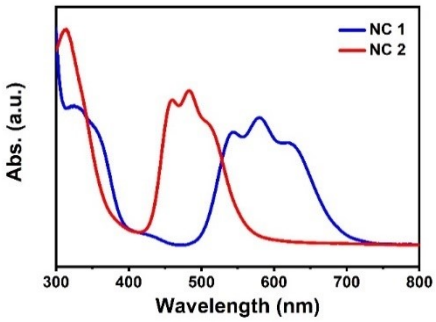

Figure S11. The absorption spectra of NCs **1** (blue) and **2** (red) in CH_2Cl_2, respectively.

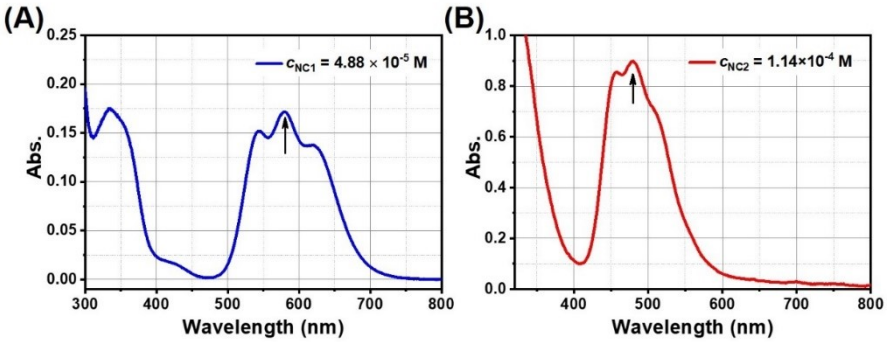

Figure S12. The molar absorptivity (ε) determined by the standard absorption curve of the isolated NC **1** and NC **2**.

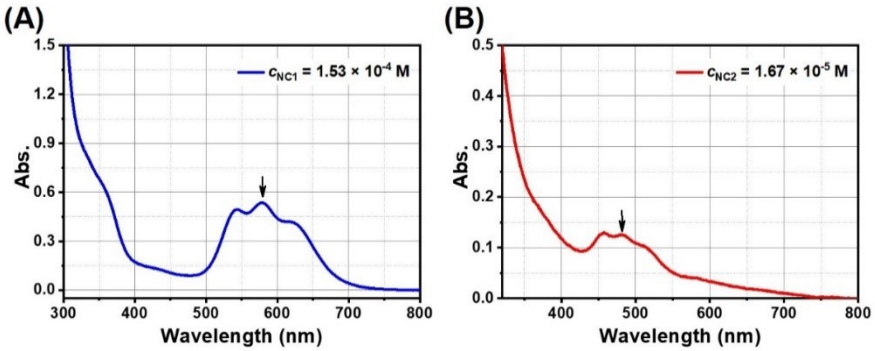

Figure S13. Absorption spectra of the reaction mixture. (A) NC **1**: 300 μL reaction sample at 12 h was diluted to 4 mL in CH_2Cl_2. (B) NC **2**: 200 μL reaction sample at 36 h was diluted to 5 mL in CH_2Cl_2.

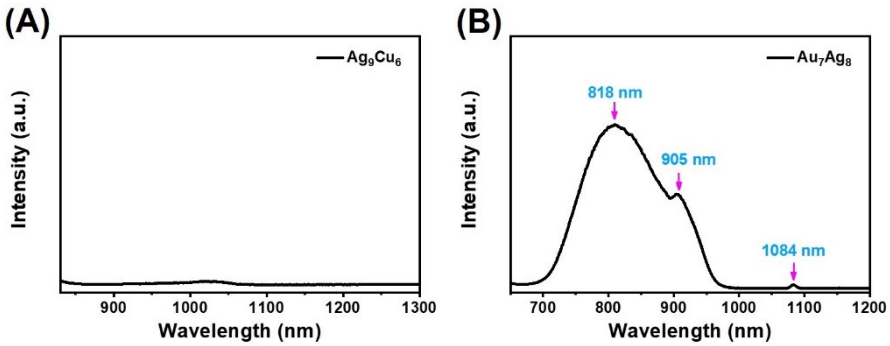

Figure S14. The emission spectra of (A) NC **1** and (B) NC **2** in dichloromethane (λ_{ex}= 580 nm for NC **1**; λ_{ex}= 482 nm for NC **2**).

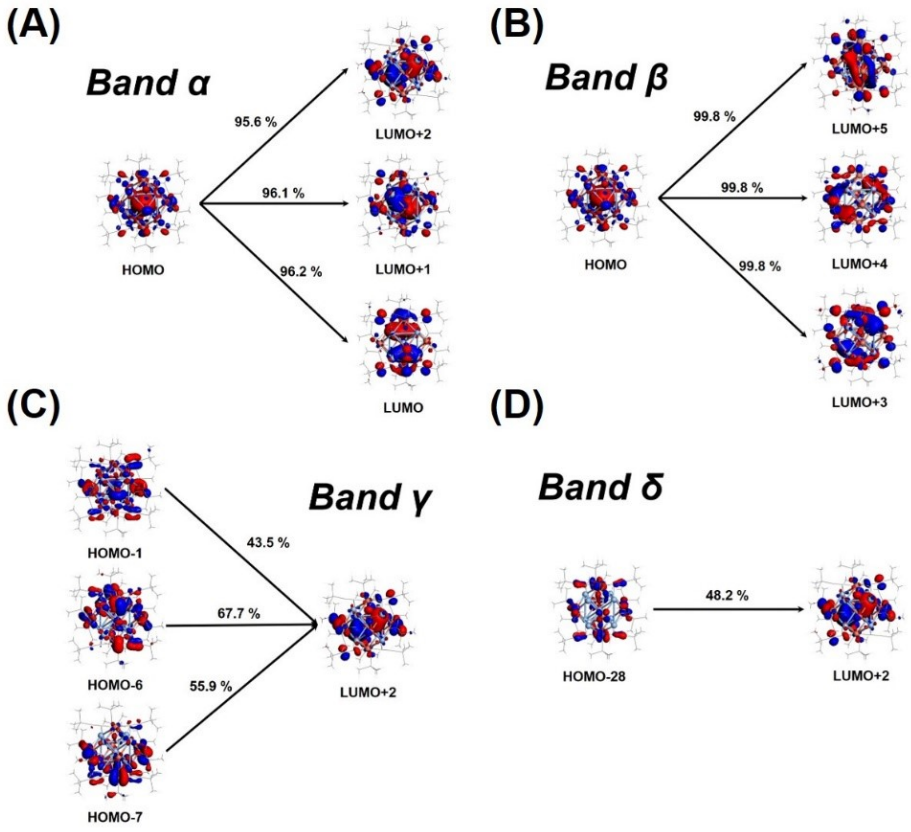

Figure S15. The main transitions corresponding to the band (A) α, (B) β, (C) γ, and (D) δ in the absorption spectrum of NC **1**. Frontier orbitals including HOMO, HOMO-1, HOMO-6, HOMO-7, HOMO-28, LUMO, LUMO+1, LUMO+2, LUMO+3, LUMO+4, and LUMO+5 of NC **1**.

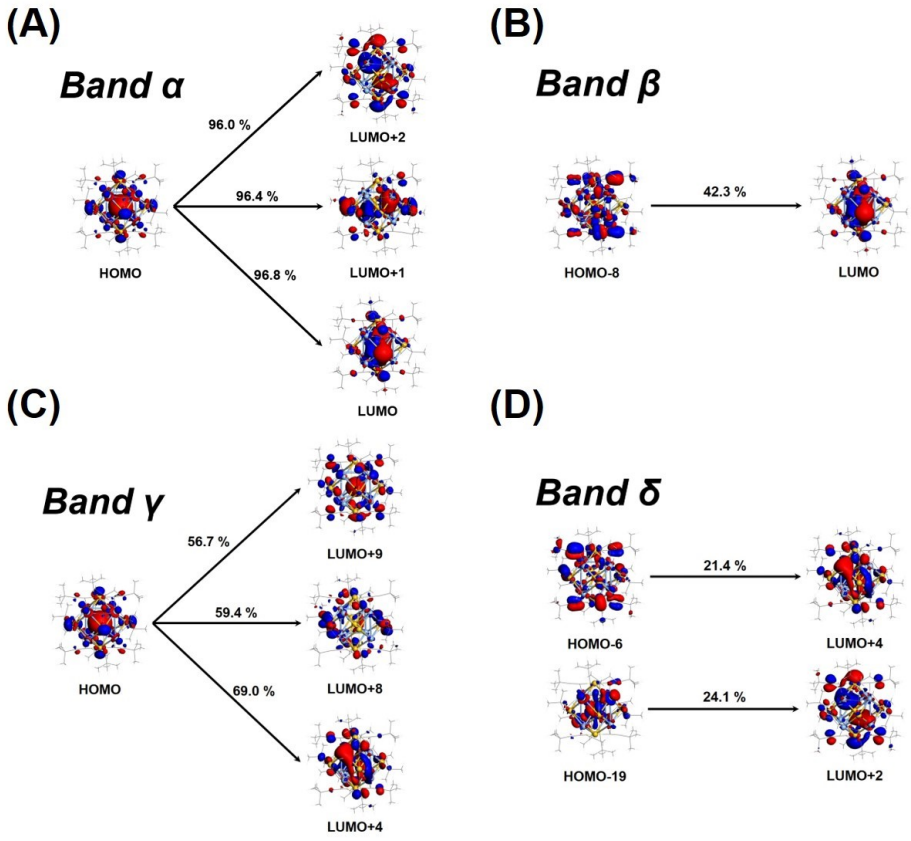

Figure S16. The main transitions corresponding to the band (A) α, (B) β, (C) γ, and (D) δ in the absorption spectrum of NC **2**. Molecular orbitals including HOMO, HOMO-6, HOMO-8, HOMO-19, LUMO, LUMO+1, LUMO+2, LUMO+4, LUMO+8, and LUMO+9 of NC **2**.

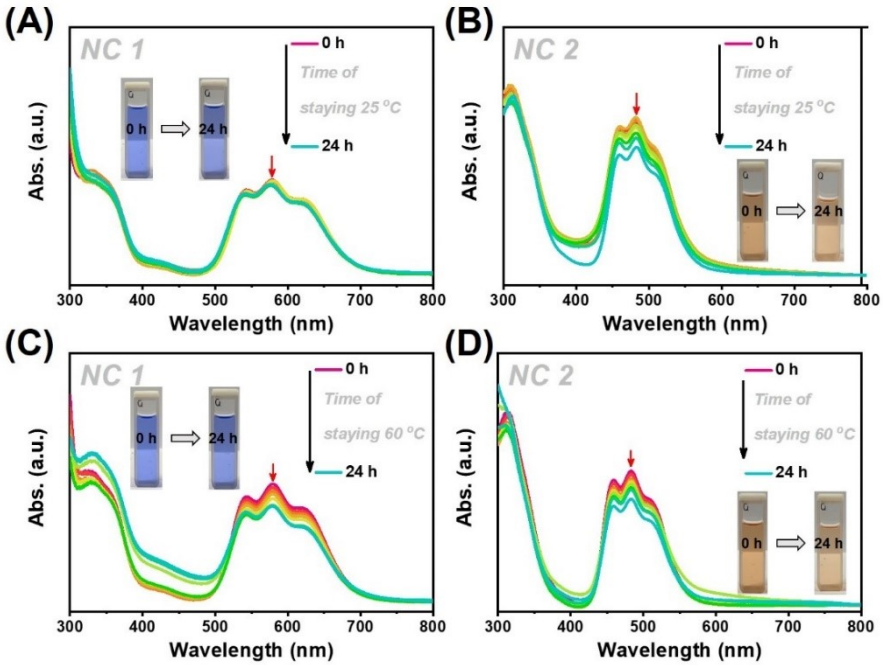

Figure S17. The stability comparison of NCs **1** and **2**. The UV-vis absorption spectra of the two NCs (0.5 mg) dissolved in 4 mL 1, 2-dichloroethane at (A), (B) room temperature**,** and (C), (D) heating to 60 °C at different times. Insert: photographs of the two NCs in 1, 2-dichloroethane at 0 h and 24 h, respectively.

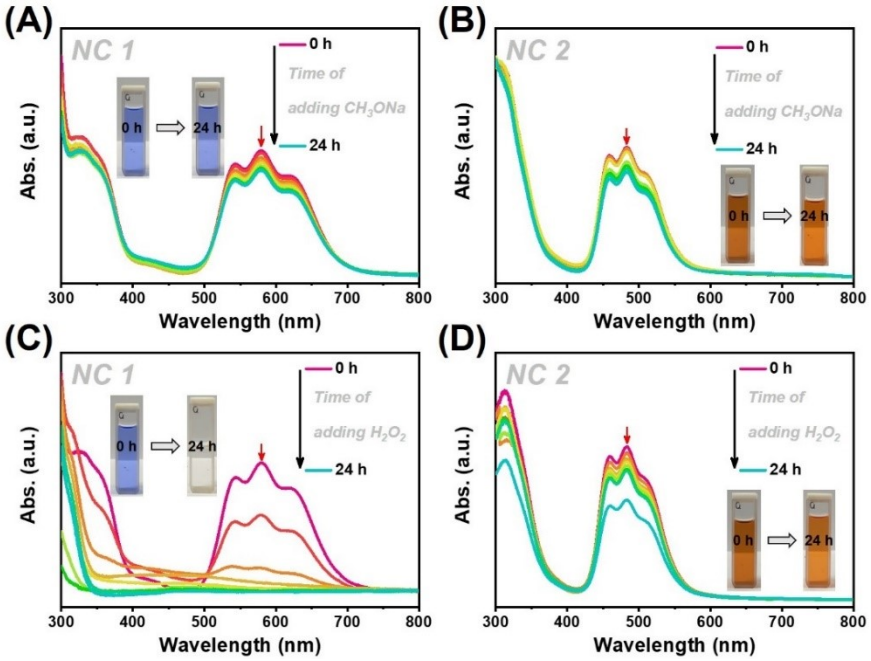

Figure S18. The stability comparison of NCs **1** and **2** in the presence of oxidative and Lewis base. The time-resolved UV−vis absorption spectra of the two NCs (1.0 mg) in 4 mL CH_2Cl_2 solution in the presence of (A), (B) H_2O_2 (30%, 30 μL), and (C), (D) CH_3ONa (0.25 mg in 250 μL ethanol). Insert: photographs of the two NCs in CH_2Cl_2 at 0 h and 24 h, respectively.

Supporting Tables

Table S1. The summary of XPS data of NCs **1** and **2**.

Sample	Ag $3d_{3/2}$ (eV)	Ag $3d_{5/2}$ (eV)	Au $4f_{5/2}$ (eV)	Au $4f_{7/2}$ (eV)	Cu $2p_{1/2}$ (eV)	Cu $2p_{3/2}$ (eV)	Atomic ratio	
							Exp.	Cal.
NC **1**	374.41	368.41	None	None	953.02	933.12	Ag/Cu= 10.33/6.90	9/6
NC **2**	374.83	368.83	88.17	84.50	None	None	Ag/Au= 8.27/7.28	8/7

Table S2. The crystal structure parameters for NC **1**.

Identification code	$[Ag_9Cu_6(C_6H_9)_{12}SbF_6]$
Empirical formula	$C_{72}H_{108}Ag_9Cu_6F_6Sb$
Formula weight	2561.35
Temperature/K	100(2)
Crystal system	Trigonal
Space group	*R*
a/Å	16.0180(2)
b/Å	16.0180(2)
c/Å	28.5069(4)
α/°	90
β/°	90
γ/°	120
Volume/Å^3	6334.28(18)
Z, Calculated density/ Mg/m^3	3.00006, 2.014
Absorption coefficient/ mm^{-1}	3.872
F(000)	3726
Crystal size/mm^3	0.04 × 0.04 × 0.06
Radiation	CuK_α (λ = 1.54184)
2θ range for data collection/°	2.543 to 30.869
Index ranges	$-22 \le h \le 22$, $-23 \le k \le 23$, $-39 \le l \le 39$
Reflections collected	37177
Independent reflections	3842 [R(int) = 0.0368]
Data/restraints/parameters	3842/ 132/ 191
Goodness-of-fit on F2	1.136
Final R indexes [I>=2σ (I)]	R_1 = 0.0731, wR_2 = 0.1722
Final R indexes [all data]	R_1 = 0.0835, wR_2 = 0.1773
Largest diff. peak/hole / e Å^{-3}	2.413/ -2.742

Table S3. The crystal structure parameters for NC **2**.

Identification code	$[Au_7Ag_8(C{\equiv}CBu^t)_{12}]SbF_6$
Empirical formula	$C_{72}H_{108}Au_7Ag_8F_6Sb$
Formula weight	3215.24
Temperature/K	100.00(10)
Crystal system	Trigonal
Space group	*R*
a/Å	21.7764(7)
b/Å	21.7764(7)
c/Å	15.3445(5)
α/°	90
β/°	90
γ/°	120
Volume/Å^3	6301.7(5)
Z, Calculated density/ Mg/m^3	3.00006, 2.542
Absorption coefficient/ mm^{-1}	6.656
F(000)	4407
Crystal size/mm^3	0.08 × 0.05 × 0.05
Radiation	CuK_α (λ = 1.54184)
2θ range for data collection/°	3.714 to 66.410
Index ranges	$-24 \le h \le 25$, $-25 \le k \le 25$, $-13 \le l \le 18$
Reflections collected	7053
Independent reflections	2396 [R(int) = 0.0513]
Data/restraints/parameters	2396 / 107 / 138
Goodness-of-fit on F^2	1.023
Final R indexes [I≥2σ (I)]	R_1 = 0.0536, wR_2 = 0.1280
Final R indexes [all data]	R_1 = 0.0712, wR_2 = 0.1382
Largest diff. peak/hole / e Å^{-3}	1.610 / -2.663

Table S4. The reported Ag-Ag distances in core and shell of alkynyl-protected homometallic and heterometallic Ag NCs.

Avg. Ag-Ag distances in core (Å)	Avg. Ag-Ag distances in shell (Å)	Structure of NCs	Molecular formula of NCs	Ref.
2.863	2.894	icosahedral Ag_{13}	$[Ag_{25}Cu_4(PhC{\equiv}C)_{12}(PPh_3)_{12}Cl_6H_8]^{3+}$	12
Not available	2.715	$Ag@Ag_{14}$	$Ag_{51}(^tBuC{\equiv}C)_{32}$	13
Not available	2.802	$Au_4@Ag_{22}$	$Ag_{74}(PhC{\equiv}C)_{44}$	14
Not available	2.980	$Au_{22}@Ag_{48}$		
Not available	2.929 ~ 3.489	anticuboctahedral Ag_{13}	$[Ag_{19}(dppm)_3(PhC{\equiv}C)_{14}]^{3+}$	15
3.02	Not available	icosahedral Ag_{13}	$[Ag_{35}(H_2L)_2(L)(^tBuC{\equiv}C)_{16}]^{3+}$ (H_4L= *p-tert*-butylthiacalix[4]-arene)	16
2.85	2.817	$Ag_{13}@Ag_{42}$	$[Ag_{112}Cl_6(ArC{\equiv}C)_{51}]^{3-}$ (Ar= 3,5-$(CF_3)_2C_6H_3$-)	1
2.928	2.927	$Ag_{42}@Ag_{48}$		
3.080	3.093	$Ag_{48}@Ag_9$		
Not available	3.273	Ag_8 cube	$[Ag_8Au_7(^tBuC{\equiv}C)_{12}]^+$	11 and this work
Not available	3.3331	Ag_8 cube	$[Ag_9Cu_6(^tBuC{\equiv}C)_{12}]^+$	This work
Not available	2.953 ~ 2.986	Ag_{14} cage	$[Ag_{14}(^tBuC{\equiv}C)_{12}Cl]^+$	17
Not available	2.9747	Ag_{14} cage	$[Ag_{14}(^tBuC{\equiv}C)_{12}]^{2+}$	17

Table S5. Absorption coefficients of NC **1** and NC **2** of **Figure S12.**

Sample	Molecular weight (M, g mol^{-1})	Wavelength (λ_{max}, nm)	Absorbance (A)	Concentration (c, M)	Absorption coefficient (ε, M^{-1} cm^{-1})
NC **1**	2561.46	580	0.17	4.88×10^{-5}	0.35×10^{4}
NC **2**	3277.37	483	0.89	1.14×10^{-4}	0.78×10^{4}

Table S6. The amounts of reactants and the product of NC **1** (at 12 h).

Amount of reactants (mol)	Concentration of sample (M)	Amount of NC **1** in reaction (mol)	Yield
0.33×10^{-5} (^{t}BuC≡CAg) 0.69×10^{-5} ($(PPh_3)_2CuBH_4$)	1.53×10^{-4}	2.04×10^{-5}	41.05% (based on Ag) 41.74% (based on Cu)

The calculation process of the yields of NC 1:

Sample:

$$c_{NC\,1} = \frac{0.536}{0.35 \times 10^{-4}\,(M^{-1}cm^{-1}) \times 1\,(cm)} = 1.53 \times 10^{-4}\,(M)$$

Reaction solution:

$$n_{NC\,1} = \frac{1.53 \times 10^{-4}\,(M) \times 4\,(mL) \times 10\,(mL)}{300\,(\mu L)} = 2.04 \times 10^{-5}\,(mol)$$

The yield of product based on Ag:

$$Y_{NC\,1} = \frac{2.04 \times 10^{-5}\,(mol) \times 37.90\%}{0.33 \times 10^{-4}\,(mol) \times 57.07\%} \times 100\% = 41.05\,\%$$

The yield of product based on Cu：

$$Y_{NC\,1} = \frac{2.04 \times 10^{-5}\,(mol) \times 14.88\%}{0.69 \times 10^{-4}\,(mol) \times 10.54\%} \times 100\% = 41.74\,\%$$

Table S7. The amounts of reactants and the product of NC **2** (at 36 h).

Amount of reactants (mol)	Concentration of sample (M)	Amount of NC **2** in reaction (mol)	Yield
$Au_{22}(^{t}BuC{\equiv}C)_{18}$	1.53×10^{-4}	1.67×10^{-5}	86.72% (based on Au)

The calculation process of the yields of NC 2:

Sample:

$$c_{NC\,1} = \frac{0.13}{0.78 \times 10^{-4}\,(M^{-1}cm^{-1}) \times 1\,(cm)} = 1.67 \times 10^{-5}\,(M)$$

Reaction solution:

$$n_{NC\,1} = \frac{1.67 \times 10^{-4}\,(M) \times 3\,(mL) \times 5(mL)}{200\,(\mu L)} = 2.04 \times 10^{-5}\,(mol)$$

The yield of product based on Au:

$$Y_{NC\,2} = \frac{1.25 \times 10^{-6}\,(mol) \times 42.07\%}{8.63 \times 10^{-7}\,(mol) \times 70.41\%} \times 100\% = 86.72\,\%$$

Table S8. The transitions corresponding to the significant peaks in the absorption spectrum of NC **1**.

Peaks	Excitation energies (eV)	Sn	Transition mode	Contributions (%)
α	1.72	1	HOMO → LUMO	96.2
		2	HOMO → LUMO + 1	96.1
		3	HOMO → LUMO + 2	95.6
β	2.22	4	HOMO → LUMO + 3	99.8
		5	HOMO → LUMO + 4	99.8
		6	HOMO → LUMO + 5	99.8
γ	2.91	28	HOMO - 7 → LUMO + 2	55.9
			HOMO - 10 → LUMO + 1	24.7
		29	HOMO - 9 → LUMO + 1	16.2
			HOMO - 8 → LUMO + 1	14.0
		30	HOMO - 6 → LUMO + 2	67.7
			HOMO - 8 → LUMO + 2	21.8
		31	HOMO - 10 → LUMO + 2	19.6
			HOMO - 2 → LUMO	17.4
			HOMO - 1 → LUMO + 1	22.8
		32	HOMO - 2 → LUMO + 1	21.0
			HOMO → LUMO + 6	10.7
			HOMO - 2 → LUMO	22.0
		33	HOMO - 10 → LUMO + 2	11.5
			HOMO - 2 → LUMO + 1	10.1
		34	HOMO - 1 → LUMO + 2	43.5
δ	3.63	124	HOMO - 28 → LUMO + 1	28.9
			HOMO - 27 → LUMO + 1	28.7
			HOMO - 29 → LUMO + 1	15.1
		127	HOMO - 6 → LUMO + 4	21.5
			HOMO - 26 → LUMO	10.2
		128	HOMO - 8 → LUMO +5	15.8
			HOMO - 10 → LUMO +4	12.3
		129	HOMO - 28 → LUMO + 2	48.2
			HOMO - 27 → LUMO + 2	36.6
		130	HOMO - 25 → LUMO + 2	19.4
			HOMO - 9 → LUMO +5	16.3
			HOMO - 6 → LUMO +5	11.7

Table S9. The transitions corresponding to the significant peaks in the absorption spectrum of NC **2.**

Peaks	Excitation energies (eV)	Sn	Transition mode	Contributions (%)
α	2.04	1	HOMO → LUMO	96.8
		2	HOMO → LUMO + 1	96.4
		3	HOMO → LUMO + 2	96.0
β	2.89	24	HOMO - 8 → LUMO	42.3
			HOMO - 8 → LUMO + 1	12.5
		26	HOMO - 6 → LUMO + 2	20.3
			HOMO - 12 → LUMO	13.9
			HOMO - 8 → LUMO	12.5
			HOMO - 4 → LUMO + 2	10.8
γ	3.22	50	HOMO → LUMO + 4	69.0
			HOMO - 16 → LUMO + 1	19.7
		52	HOMO→LUMO + 8	59.4
			HOMO - 15 → LUMO	13.0
		53	HOMO → LUMO + 9	56.7
			HOMO → LUMO + 7	28.6
δ	3.66	88	HOMO - 19 → LUMO + 2	24.1
			HOMO - 6 → LUMO + 4	21.4
		89	HOMO - 3 → LUMO + 5	20.0
			HOMO - 5 →LUMO + 4	13.3
			HOMO - 2 → LUMO + 4	11.2
		90	HOMO - 7 → LUMO + 5	19.0
			HOMO - 7 → LUMO + 4	18.8
			HOMO - 8 → LUMO + 4	10.0

Table S10. The vibration frequency of NCs **1** and **2**.

NC **1**		NC **2**	
Frequency (cm^{-1})	Intensity ($km \cdot mol^{-1}$)	Frequency (cm^{-1})	Intensity ($km \cdot mol^{-1}$)
10.94	18.19	10.5	0.44
21.02	12.79	16.9	2.24
25.87	3.08	18.3	2.4
27.54	2.38	20.1	2.32
28.29	2.34	23.4	0.52
30.08	8.61	24.8	7.98
31.52	3.2	27.4	1.09
32.63	5.64	27.8	1.04
33.03	9.89	29.4	3.07
33.82	7.06	29.6	7.71
36.6	1.75	31.9	2.9
36.84	1.75	32.2	0.52

References

1. F. Hu, J. J. Li, Z. J. Guan, S. F. Yuan and Q. M. Wang, *Angew. Chem., Int. Ed.*, 2020, **59**, 5312-5315.
2. X. Ma, G. Ma, L. Qin, G. Chen, S. Chen and Z. Tang, *Sci. China Chem.*, 2020, **63**, 1777-1784.
3. G. M. Sheldrick, *Acta Crystallogr. Sect. A: Found. Adv.*, 2015, **71**, 3-8.
4. G. M. Sheldrick, *Acta Crystallogr. Sect. C: Struct. Chem.*, 2015, **71**, 3-8.
5. O. V. Dolomanov, L. J. Bourhis, R. J. Gildea, J. A. K. Howard and H. Puschmann, *J. Appl. Crystallogr.*, 2009, **42**, 339-341.
6. B. Delley, *J. Chem. Phys.*, 1990, **92**, 508-517.
7. B. Delley, *J. Chem. Phys.*, 2000, **113**, 7756-7764.
8. J. P. Perdew, K. Burke and M. Ernzerhof, *Phys. Rev. Lett.*, 1996, **77**, 3865-3868.
9. A. Tkatchenko and M. Scheffler, *Phys. Rev. Lett.*, 2009, **102**, 073005.
10. *Journal*, 2010.
11. Y. Wang, H. Su, L. Ren, S. Malola, S. Lin, B. K. Teo, H. Hakkinen and N. Zheng, *Angew. Chem., Int. Ed.*, 2016, **55**, 15152-15156.
12. H. Shen, Y. Z. Han, Q. Wu, J. Peng, B. K. Teo and N. Zheng, *Small Methods*, 2020, **5**, 2000603.
13. G. X. Duan, L. Tian, J. B. Wen, L. Y. Li, Y. P. Xie and X. Lu, *Nanoscale*, 2018, **10**, 18915-18919.
14. M. Qu, H. Li, L. H. Xie, S. T. Yan, J. R. Li, J. H. Wang, C. Y. Wei, Y. W. Wu and X. M. Zhang, *J. Am. Chem. Soc.*, 2017, **139**, 12346-12349.
15. S. F. Yuan, P. Li, Q. Tang, X. K. Wan, Z. A. Nan, D. E. Jiang and Q. M. Wang, *Nanoscale*, 2017, **9**, 11405-11409.
16. Z. J. Guan, J. L. Zeng, Z. A. Nan, X. K. Wan, Y. M. Lin and Q. M. Wang, *Sci. Adv.*, 2016, **2**, e1600323.
17. D. Rais, J. Yau, D. M. P. Mingos, R. Vilar, A. J. P. White and D. J. Williams, *Angew. Chem., Int. Ed.*, 2001, **40**, 3464-3467.